CrystEngComm

Accepted Manuscript

ROYAL SOCIETY OF CHEMISTRY

www.rsc.org/crystengcomm

Persistence of C–H…π(chelate ring) interactions in the crystal structures of palladium bis(*O*-alkyldithiocarbonate)s, $Pd(S_2COR)_2$. The utility of $Pd(S_2COR)_2$ as precursors for palladium sulphide materials†

Yee Seng Tan,[a] Siti Nadiah Abdul Halim,[a] Kieran C. Molloy,[*b] Anna L Sudlow,[b] A. Otero-de-la-Roza[*c] and Edward R.T. Tiekink*[a,d]

[a] *Department of Chemistry, University of Malaya, 50603 Kuala Lumpur, Malaysia*

[b] *Department of Chemistry, University of Bath, Bath BA2 7AY, UK. E-mail: kcm68win@outlook.com*

[c] *National Institute for Nanotechnology, National Research Council of Canada, 11421 Saskatchewan Drive, Edmonton, Alberta, Canada T6G 2M9. E-mail: alberto.oterodelaroza@nrc-cnrc.gc.ca*

[d] *Centre for Crystalline Materials, Faculty of Science and Technology, Sunway University, 47500 Bandar Sunway, Selangor Darul Ehsan, Malaysia. E-mail: edwardt@sunway.edu.my; Fax: +60 3 7491 8633; Tel: +60 3 7491 7528*

† Electronic supplementary information (ESI) available: CCDC reference numbers, 1058645-1058656. For ESI (for characterisation data, diagrams illustrating molecular structures and supramolecular aggregation) and crystallographic data in CIF format see DOI:

Abstract

The crystallographic structures of 12 palladium xanthates, $Pd(S_2COR)_2$ (R = alkyl) show a uniform adoption of square-planar PdS_4 geometries. Supramolecular aggregation in **1** (R = Me), **2** (Et) and **3** (*n*-Pr) is based on secondary Pd···S interactions, which are "turned off" when the bulk of R increases. In **4** (*i*-Pr), C–H···S hydrogen bonding is present. In each of **2**–**4**, C–H…π(PdS_2C) interactions are incorporated within the architecture, stabilised by Pd…S secondary- or C–H···S hydrogen- bonding. In **5**–**12** (R = *n*-Bu, *i*-Bu, *n*-Pent, *i*-Pent, neoPent, *n*-Hex, *i*-Hex, neoHex), varying numbers of stand-alone C–H…π(PdS_2C) interactions involving different hydrogen donors uniformly stabilise supramolecular chains in their crystal structures. In order to determine the relative importance of the various intermolecular interactions and packing effects, a computational study using dispersion-corrected density-functional theory was performed on **3** (R = *n*-Pr). The results showed that the most significant contributors to the stability of the crystal structure are Pd···S interactions followed closely by C–H···π(PdS_2C) interactions. Two non-specific hydrophobic interactions also contribute to the overall packing to a lesser extent. The utility of $Pd(S_2COR)_2$ to function as synthetic precursors for PdS nanoparticles and thin films was also investigated. Aerosol-assisted-CVD on representative examples generated PdS films with either matted, needle-like or granular morphologies depending on temperature and substrate. Solvothermal (ethylene glycol) decomposition generated sulphur-rich PdS nanoparticles with diameters 120 nm (**7** and **10**) – 400 nm (**8**). When dodecanethiol was employed as a capping agent, $PdS_{1.75}$ nanoparticles < 10 nm were generated from **1**.

Introduction

The 1,1-dithiolates are a class of uninegative ligands comprising dithiocarbamates, dithiocarbonates (hereafter, xanthates) and dithiophosphates, Scheme 1a-c.[1] Transition metal and main group element complexes of these ligands have been thoroughly studied over the years and have been the subject of several bibliographic reviews.[2] The wide application of dithiocarbamate complexes in the generation of coordination polymers is precluded by their propensity to be stabilised by the canonical structure shown in Scheme 1d, which may contribute up to 40% to the overall resonance structure.[2a,b] The adoption of this canonical structure has two effects. Firstly, dithiocarbamates prove to be very effective chelating agents with the consequence they have a reduced tendency to bridge, compared with xanthates and dithiophosphates.[3] Secondly, the enhanced donation of electrons to the metal centre reduces the Lewis acidity of the latter which in turn diminishes the likelihood of the formation of additional coordinate bonds to, for example, bridging bipyridine-type ligands, ubiquitous in coordination polymers.[4] Conversely, the enhanced metalloaromatic[5a,b] behaviour of chelate rings formed by dithiocarbamate ligands enables the formation of C–H$\cdots\pi$(chelate ring) interactions in their crystal structures. The importance of metalloaromaticity in this context notwithstanding, it needs to be stated that analogous C–H$\cdots\pi$ interactions can and do occur in non-aromatic systems.[5c-e]

For 1,1-dithiolate compounds, C–H$\cdots\pi$(MS_2C) interactions, where MS_2C represents the four-membered chelate ring, were possibly first noted in the crystal structures of cadmium(II) bis(xanthates) adducts[6a] and subsequently identified in a range of transition metal and main group element bis(1,1-dithiolate) analogues.[6b-d] These latter bibliographic surveys showed C–H$\cdots\pi$(MS_2C) interactions occur most frequently in dithiocarbamates compared with other 1,1-dithiolates, which is consistent with significant π-character in the chelate rings formed by these

ligands, owing to the marked contribution of the canonical structure shown in Scheme 1d, certainly compared with the analogous structure shown in Scheme 1e for the xanthate anion. Also, C–H···π(MS_2C) interactions were noted to appear independently of other readily identifiable intermolecular interactions to sustain zero-, one-, two- and three-dimensional architectures, with chains and layers being dominant.[6d] A variety of other chelate rings are also known to participate in analogous C–H···π(MS_2C) interactions,[7] for instance, chelate rings formed by acetylacetonate and derivatives in square planar transition metal complexes have been extensively studied.[8] Zarić *et al*.[8] estimate that the energy of association of C–H···π(MO_2C_2) is in the range 6-11 kJ mol^{-1} which is comparable to that for C–H···π(arene) of 1-8 kJ mol^{-1} in organic structures.[9]

In the original survey of the prevalence of C–H···π(MS_2C) interactions in metal/main group bis(1,1-dithiolate)s, for xanthate derivatives it was noted that i) the shortest H···ring centroid(MS_2C) separation was observed in the crystal structure of Pd(S_2CO-*i*-Pr)$_2$[10a] and ii) a relatively large number of nickel(II) xanthate complexes exhibited C–H···π(NiS_2C) interactions.[6d] In this context, it was thought of interest to evaluate the propensity of C–H···π(PdS_2C) interactions in the crystal structures of a series of Pd(S_2COR)$_2$ complexes, *i.e*. **1**–**12** (Scheme 2).

Palladium xanthates have been investigated previously owing to an interest in developing non-platinum based anti-cancer agents[10b] and to investigate their utility as synthetic precursors for the generation of PdS nanocrystals.[10a] Several crystal structures are available for Pd(S_2COR)$_2$ complexes, namely R = Me,[10a,c] Et,[10d,e] *i*-Pr,[10a] CH_2CF_3[10f] and 2,4,6-trimethylphenyl.[10g] Herein, the crystal structures of **1**–**12** are described, their crystal packing patterns analysed and theoretical methods employed to estimate the energy of attraction associated with a C–H···π(PdS_2C) interaction. Finally, the utility of Pd(S_2COR)$_2$ complexes as

molecular precursors for the generation of palladium sulphide nanoparticles and thin films has been evaluated.

Results and discussion

Complexes **1**–**12** (see Scheme 2) were prepared in crystalline form in good yields. Full details of synthesis and characterisation are given in ESI Tables S1-S12. Allowing for differences in composition, there is significant homogeneity in the spectroscopic characteristics. The key results of the characterisation relate to the narrow range of the chemical shifts due to $S_2\underline{C}O$ in the $^{13}C\{^1H\}$ NMR, *i.e.* 232.7- 234.7 ppm, and the similarity of these to the equivalent chemical shifts for the respective uncoordinated xanthate anions (recorded in D_2O) indicating a high degree of delocalisation of π-electron density over the PdS_2C atoms. The UV/vis spectra were also very similar to each other, consistently exhibiting four absorptions.[11] Two intense high-energy bands in the narrow ranges 236-238 and 282-285 nm are assigned to metal-ligand charge-transfer n → σ* and intra-ligand π → π* transitions, respectively. Weaker ligand-metal charge-transfer (CT, n → π*) bands are observed in the range 378-381 nm, and even weaker *d-d* ($^1A_{1g}$ → ^1E_g) transitions occur in the range 448-461 nm. In order to confirm these assignments, Gaussian[12] calculations were run to confirm the source of the observed electronic transitions. The UV/vis spectrum for the optimised molecule in **3** (R = *n*-Pr), see ESI Fig. S1a, was calculated using time-dependent DFT. The geometry was relaxed using B3LYP/6-31+G(d,p)[13a,b] except for Pd, for which aug-cc-pVDZ-PP[13c] was used. Sixty singlet-singlet vertical transitions were calculated. A polarizable continuum model (PCM)[13d] was used in order to reproduce the effects of the solvent (acetonitrile). The resulting spectrum is shown in ESI Fig. S1b, which was calculated using the Gausssum program.[13e] The calculated high-energy transitions have

wavelengths of 286.4 nm and 224.3 nm, in good agreement with the experimental values (284 nm and 237 nm, respectively). The most intense absorption (284 nm) can be clearly identified as being derived from the π-orbitals in the chelate (PdS_2C) ring. The remaining transitions, including the one at 237 nm, involve charge transfer excitations between Pd and the xanthate ligands.

The NMR and UV/vis data suggest the xanthate ligands have a very similar electronic profile which is independent of the alkyl group and consistent with the results of their geometry-optimised structures.[14] In keeping with the above, the molecular structures of **1**–**12** are also very similar. The structures of **1**, **2** and **4** have been described previously.[10a, c-e] New data for these complexes are now reported here, recorded at low temperature and under similar experimental conditions for the complete series, in order to obtain a consistent data set over 12 structures. Complex **1** has been described twice,[10a,c] and the new results are consistent with these. The structure of **2** has been described in both centrosymmetric *Pbca*[10d] and non-centrosymmetric $Pca2_1$;[10e] the centrosymmetric model is employed herein. Finally, the original report[10a] of the structure of **4** is matched by the new determination.

Molecular structures

The molecular structure of **8**, being an exemplar of the remaining $Pd(S_2COR)_2$ structures, is illustrated in Fig. 1; illustrations of all molecular structures are given in ESI Tables S1-S12. The asymmetric unit of each of **1** and **3** comprises an entire molecule, whereas the Pd atom in the remaining structures is located on a centre of inversion. In each of **1**–**12** the Pd atom is chelated by two xanthate ligands which define a square planar geometry. Selected interatomic parameters are collated in ESI Table S14 from which it can be seen that the range of Pd–S bond lengths is

narrow, *i.e.* 2.3210(6)-2.3432(15) Å, indicating that the xanthate ligands are symmetrically chelating, as indicated by the solution spectroscopy. Reflecting this is the experimental equivalence of the associated C–S bond lengths, which lie in the range 1.693(5)-1.706(3) Å. In spite of the similarity in the molecular structures, disparate crystal packing patterns are observed, as discussed below.

Supramolecular structures

Complexes **1-12** crystallise in five different crystal packing patterns that can be roughly divided into those structures that exhibit intermolecular Pd···S or C–H···S interactions and those that do not. In **1** (R = Me), with no crystallographically imposed symmetry in the molecule, centrosymmetrically related molecules are connected into dimeric aggregates by Pd···S1^{i} secondary interactions,[15] Fig. 2a; symmetry operation: 1-*x*, 2-*y*, 1-*z*. The Pd···S1^{i} separation of 3.3165(13) Å is within the sum of the van der Waals radii of Pd (1.63 Å) and S (1.80 Å), *i.e.* 3.43 Å.[16a] Molecules assemble into layers that stack along the *b*-axis with no directional interactions between them in accord with the criteria embodied in PLATON;[17] see ESI Fig. S2. However, it is noted that there are weak S1…S2^{ii} interactions of 3.6206(18) Å, which are just beyond the sum of the van der Waals radii for sulphur, that assemble dimeric aggregates into rows along the *a*-axis; *ii*: -1+*x*, *y*, *z*. The second species without crystallographically imposed symmetry is **3** (R = *n*-Pr). These, too, assemble into centrosymmetric dimeric aggregates *via* Pd···S2^{i} secondary interactions of 3.3678(9) Å; *i*: 2-*x*, 1-*y*, 1-*z*. As shown in Fig. 2b, two other noteworthy features of the crystal packing are highlighted. Firstly, within the dimeric aggregates there are methylene-C–H···π(PdS$_2$C) interactions, Table 1. As noted in the original bibliographic reviews of these types of interaction,[6c,d] the geometric parameters characterising these appear in the

PLATON[17] output as possible examples of C–H···π interactions. The connections between dimeric aggregates leading to supramolecular chains aligned along the *a*-axis are anagostic[18] methylene-C–H···Pd interactions, Table 1, so that the methylene acts a bridge between two adjacent molecules in the chain. This type of interaction is attracting increasing attention in the structural chemistry of metal 1,1-dithiolates owing largely to the work of Singh *et al*.[19] The chains pack in the crystal structure separated by hydrophobic interactions, ESI Fig. S3.

At this point, it is worthwhile to consider the C–H···π(PdS_2C) and Pd···H interactions in the context of their van der Waals radii. For the putative C–H···π(PdS_2C) interactions, the van der Waals radius of the chelate ring is taken as 1.90 Å, being the value accepted as the half-thickness of a phenyl ring, based on the upper value estimated for half the separation between the two centroids in parallel phenyl rings.[16b] Thus, adding this to 1.20 Å, the Bondi van der Waals radius for hydrogen,[16a] the sum of the van der Waals radii becomes 3.10 Å. However, if the widely accepted value of 1.09 Å[16c] is used for a hydrogen atom, the sum of the van der Waals radii reduces to 2.99 Å. In searching for C–H···π(MS_2C) and allied M(lp)…π(phenyl)[20] interactions in the Cambridge Crystallographic Database (CSD),[21] 10% of the value of the sum of the van der Waals radii is usually added in order to capture all possible interactions, a practice which seems to be widely accepted as there is no absolute cut-off for a putative interaction.[22] Therefore, the C–H···π(PdS_2C) contacts in **3** clearly fall within the sum of the van der Waals radii of the interacting species. Concerning the Pd···H interactions, the sum of the van der Waals radii for palladium[15a] and hydrogen (1.09 Å)[15c] is 2.72 Å, a value shorter than 2.83 Å for the C–H···Pd interaction in **3** but well within the sum of the van der Waals radii + 10% criterion.

As mentioned earlier, the remaining molecular structures are centrosymmetric. In **2** (R = Et), supramolecular layers are formed in the *ab*-plane sustained by Pd···S interactions (3.3612(6) Å; 1/2+*x*, 3/2-*y*, 1-*z*) above and below the square plane, Fig. 2c. Within this framework are methylene-C–H···π(PdS_2C) interactions, Table 1, with, from symmetry, each chelate ring participating in one such contact. Layers stack along the *c*-axis being separated by hydrophobic interactions, ESI Fig. S4.

In keeping with the well-established principle in structural chemistry of metal 1,1-dithiolates, namely that increasing the steric bulk of the R group will "turn-off" secondary M···S interactions,[23] branching in **4** (R = *i*-Pr) and increasing size in **5-12** leads to crystal packing patterns devoid of Pd···S interactions. In **4**, C–H···S interactions cooperate with methine- and methyl-C–H···π(PdS_2C) interactions to generate a supramolecular layer parallel to (-1 0 1), Fig. 2d. In all there are four C–H···π(PdS_2C) interactions per molecule. Layers pack with no directional interactions between them, ESI Fig. S5.

The structures of **5-12** exhibit the same global crystal packing patterns with each featuring C–H···π(PdS_2C) interactions operating independently of other recognisable supramolecular synthons leading to supramolecular chains. While the crystal packing of **5** also features C–H···S interactions, which link chains, those of **6-12** do not. In fact, no other recognisable intermolecular synthons are apparent in **6-12**. Despite these similarities and the fact that all molecules are centrosymmetric, crystallising with half a molecule in the asymmetric unit in the triclinic ($P\bar{1}$) space group, the mode of association between molecules *via* C–H···π(PdS_2C) interactions is not consistent across the series with five different supramolecular motifs discerned. These are now discussed below in terms of complexity of modes of association.

The simplest mode of association between molecules based on C–H···π(PdS_2C) interactions leading to supramolecular chains is found in the crystal packing of **9** (R = neoPent) where methylene-C–H···π(PdS_2C) interactions, one per chelate ring, on opposite sides of the molecule from symmetry, link molecules into chains aligned along the *b*-axis, Fig. 3a and Table 1. As for all other supramolecular chains described below, the chains in **9** pack with no directional interactions between them, Fig. S6. In **5** (R = *n*-Bu), supramolecular rows of molecules aligned along the *b*-axis are sustained by four methylene-C–H···π(PdS_2C) interactions per molecule, Fig. 3b. These are connected into layers by C–H···S hydrogen bonds that stack along the *c*-axis, being separated by hydrophobic interactions, ESI Fig. S7. The other two structures with straight alkyl chains, *i.e.* **7** (R = *n*-Pent), and **10** (R = *n*-Hex), exhibit the same patterns of 1,3-methylene-C–H···π(PdS_2C) supramolecular association as for **5**, ESI Figs S8 and S9. A similar aggregation is found for **11** (R = *i*-Hex) where branching occurs at the penultimate carbon, ESI Fig. S10. The mode of association for **8** (R = *i*-Pent) is as just described for **5** but, with the hydrogen atoms derived from 1,4-related methylene- and methyl-hydrogens, Fig. 3c and ESI Fig. S11. The aggregation in **6** (R = *i*-Bu) leading to chains aligned along the *a*-axis resembles that seen for **9** but there are two contacts per chelate ring instead of one, involving 1,3-related methylene- and methyl-hydrogen atoms, Fig. 3d and ESI Fig. S12. Finally, in **12** (R = *neo*-Hex), chains are formed along the *b*-axis with six C–H···π(PdS_2C) interactions per molecule. Here, 1,2-related methylene hydrogens span two chelate rings, with the oxygen-bound methylene interacting with one chelate ring, and both methylene hydrogen atoms interacting with the other chelate ring on the same side of the PdS_4 square-plane, Fig. 3e and ESI Fig. S13.

A common feature of the aggregation patterns involving C–H···π(PdS_2C) interactions, when formed, is the participation of an oxygen-bound methylene hydrogen atom in all examples

except in **9**, Fig. 3a, where steric pressures presumably preclude the close approach of this group. This observation is consistent with the notion that these hydrogens would be the most acidic in these molecules. An evaluation of the data included in Table 1 suggests no correlations between the H···centroid(PdS_2C) distance and the nature of the hydrogen atom participating in a C–H···π(PdS_2C) interaction nor between these distances and the angles subtended at the hydrogen atom. This lack of correlation is not unexpected for weak interactions.[6c,d,24]

Computational study

As noted above and illustrated in Fig. 2b, the crystal packing of **3** (R = *n*-Pr) features secondary Pd…S as well as methylene-C–H···π(PdS_2C) and methylene-C–H···Pd interactions. This structure was therefore chosen for a computational study in order to delineate the importance and nature of these interactions. Several calculations were conducted for this study. First, the experimental crystal geometry was relaxed using DFT, corrected using the exchange-hole dipole moment (XDM) model.[25a,b] The XDM dispersion energy has been shown to efficiently represent the intermolecular interactions in molecular crystals[26a] and in the gas-phase,[26b] particularly in systems involving transition metals.[26c] XDM has shown to provide excellent accuracy for non-covalent interactions occurring between metal complexes bound by metallophilic effects.[26c] These results, combined with the non-empirical nature of the dispersion co-effcients in XDM, makes it an ideal protocol for the study of the intermolecular interactions in palladium xanthates presented in this work. For the crystal structure, the calculations were carried out using Quantum ESPRESSO,[27a] and the XDM correction was coupled with the B86BPBE exchange-correlation functional.[27b,c] The plane-wave energy cut-off was 60 Ry and the density cut-off was 600 Ry. A 4 x 4 x 4 k-point grid was used. The lattice energy, of **3** was calculated by relaxing

the molecule inside a supercell with 50 Bohr cell length. The equilibrium crystal structure shows a cell volume of 642.4 Å and a lattice energy of 141.83 kJ/mol per molecule. This lattice energy is relatively high, compared to molecules of roughly the same size,[25b] especially considering there are no strong hydrogen bonds or other directional interactions, *e.g*. halogen.

At the converged crystal geometry, the B86BPBE electron density was obtained and the non-covalent interaction (NCI) plots[26a,b] were calculated for the relevant intermolecular contacts using the Critic2 program.[27] There are four non-equivalent contacts in the crystal structure of **3**: a) a stacked contact involving two methylene-C–H···π(PdS_2C), b) a stacked contact with two Pd···S interactions, and two distinct side-by-side intermolecular contacts involving mostly the aliphatic substituents (c and d); these are illustrated in Fig. 4.

The NCI plots shows that the dominant contributions to the lattice energy, in order of relative importance, come from the Pd···S interactions, the methylene-C–H···π(PdS_2C) contacts followed by the hydrophobic contacts. While the latter contributions are not specific and likely originate from dispersion, as evidenced by the low-density extensive NCI regions, the two types of secondary contacts, *i.e*. Pd···S and C–H···π(PdS_2C), are directional and give localised high-density NCI domains. It is important to notice the high efficiency of the molecular packing in this crystal structure. The green NCI domains in Figs 4c and d follow the hydrophobic surface of the molecules in contact, indicating that the bumps and hollows match between molecules.

In order to estimate the relative contributions to the lattice energy from each of the four intermolecular contacts in the crystal, the binding energies in the gas-phase of the four dimers shown in Fig. 4 were calculated. These four dimers constitute the nearest-neighbour intermolecular contacts in the crystal. The dimers were frozen at the crystal geometry. The

calculations were run using Gaussian,[12] the LC-wPBE-XDM functional,[28a-c] and the pc-2-spd basis set.[28c] The latter is particularly well-suited for the calculation of non-covalent interactions.[28b] For the Pd atom, the basis-set/pseudopotential combination aug-cc-pVDZ-PP[13c] was employed. Referring to Fig. 4, the calculated binding energies were: (a) 62.9, (b) 67.4, (c) 29.9 and (d) 20.9 kJ/mol. The NCI plots in Fig. 4 show that dimers (a) and (b), which are much more strongly bound than the other two, contain a C–H···π(PdS_2C) and Pd···S interaction, respectively. Thus, the binding energies for the dimers at the crystal geometry suggest that the directional Pd···S and C–H···π(PdS_2C) contacts are the main contributors to the stability of the crystal structure, and that the Pd···S interaction is marginally stronger than C–H···π(PdS_2C).

However, the contribution from the two hydrophobic contacts (c and d) is by no means negligible, which explains the disparate crystal packing observed for the other crystals (**1**, **2**, **4**-**12**). For the crystal structures involving larger substituents, it is expected that global crystal packing effects will become more important, eventually overcoming the Pd···S and C–H···π(PdS_2C) contributions and therefore, controlling the crystal structure. Finally, it is also observed that the relaxation energy for the monomer of **3** from its conformation in the crystal structure to its equilibrium gas-phase structure is 14.15 kJ/mol, with minor changes on the orientation of the substituents upon relaxation so that all the non-H atoms are strictly co-planar, see the overlay diagram ESI Fig. S1.

Utility of $Pd(S_2COR)_2$ as precursors for PdS materials

Relatively few reports have dealt with the generation of palladium sulphide, either as nanoparticles or in thin film form, from molecular precursors. By far the most studied group of

compounds are palladium(II) dithiocarbamates, which have been the focus of most chemical vapour deposition (CVD) studies. Homoleptic $Pd(S_2CNR^1R^2)_2$ [$R^1 = R^2$ =Et;[29a] R^1 = Me, R^2 = Et,[29a] *n*-Bu[29a] *n*-Hex[29a,b]] generate films of a variety of stoichiometries (Table 2). In general, film deposition occurs at T > 450 ^oC and despite the Pd:S ratio of 1:4 in the precursor, the films deposited show stoichiometries which are commonly palladium-rich, with Pd^0 seen in one case at a deposition temperature of 525 ^oC.[29a] By contrast, the heteroleptic organopalladium dithiocarbamate, [(η^3-C_3H_5)Pd(S_2CNMeHex)], with a Pd:S of only 1:2, affords palladium-rich films at a lower temperature (350 ^oC; Table 2).[29c] The exception to these observations is $Pd[S_2CN(Me)Hex]_2$ which deposits PdS at the high temperature of 500 ^oC,[29a] while the dithio-imidodiphosphinato complex, $Pd[N(i\text{-}Pr_2PS)_2]_2$, surprisingly deposits PdS_2 at 500 ^oC, though this is possibly not phase-pure.[29d] The closest study to the one reported here describes the deposition of PdS at 300 ^oC by low-pressure CVD, or at an even lower temperature when photo-assisted (Table 2), using the xanthate complex, $Pd(S_2CO\text{-}i\text{-}Pr)_2$.[29e] In all, these reports collectively support an early observation that the stoichiometry of palladium sulphide phases is highly temperature dependent.[29f]

Only two studies deal with the formation of palladium sulphide nanoparticles from molecular precursors. Decomposition of $Pd[S_2CN(Me)Hex]_2$ in TOP / TOPO at 250 ^oC gave TOPO-capped PdS nanoparticles of average diameter 48.7 Å.[29b] In contrast, Na_2PdCl_4 powder and excess octylamine in high-boiling 4-*t*-butyltoluene formed only Pd nanoparticles, though when dodecanthiol was added sulphurised-Pd nanoparticles were produced along with the complex $[Pd(SC_{12}H_{25})_2]_6$.[29g] However, when this latter species was itself used as a single-source precursor, monodisperse PdS nanoparticles 2.87 ± 0.51 nm in diameter, protected by a layer of thiolate species on the surface, were produced.[29h]

Aerosol-assisted CVD has been explored using **2**, **5**, **6** and **12** as precursors, representing short-, branched- and long-alkyl chain derivatives. As the results from each precursor are broadly the same the discussion will focus mainly on results from **2**, with some general comments for the series added. Deposition from **2** at 350 ^{o}C yielded thin films of PdS on both microscope slides and silicon. In the case of the slides, both matt and a shiny areas of film were seen, though EDX shows both have the same composition ($PdS_{1.15}$ and $PdS_{1.0}$, respectively); on silicon, only a matt film of composition $PdS_{1.08}$ is seen. The difference in appearance is due to morphology, with the matt region arising from a matted, needle-like morphology (Fig. 5a), while the shiny, reflective films arise from a more powdery, granular surface (Fig. 5b). Deposition at 400 ^{o}C gives similar results: on microscope slides there is a matt grey area ($PdS_{1.02}$) and a shiny reflective part ($PdS_{0.98}$) which have similar morphologies to the films at 350 ^{o}C but with the shiny area being less dominant. There appears to be some loss of sulphur and an increase in crystallinity (less reflective, more matt in appearance) for the film with increasing temperature. However, with the exception of the shiny film deposited on slides at 350 ^{o}C from precursor **6** ($PdS_{1.0}$), none of the films gave discernible PXRD patterns. In the one positive instance, the pattern could be indexed to the major reflections of PdS (Fig. 5c; PDF 78-0206).

Solvothermal decomposition of precursors **7**–**10** in boiling ethylene glycol each generated sulphur-rich palladium sulphide nanoparticles (**7**: $PdS_{1.35}$; **8**: $PdS_{1.42}$; **9**: $PdS_{1.66}$; **10**: $PdS_{1.39}$); none of these gave PXRD patterns to allow phase identification. In the cases of **7** and **10**, uniform nanoparticles of *ca* 120nm in diameter were seen (typified by Fig. 6a), while for **9** some spheres of *ca* 160 nm are visible, the product is dominated by larger particles (*ca* 480 nm diameter). The largest particles were seen from **8**, where spheres of *ca*. 400nm dominate, with some aggregating further to *ca* 1.4μm (Fig. 6b). In contrast, when **1** was decomposed in

ethylene glycol with dodecanthiol added as capping agent (following the approach of Yang *et al.*[29g]) very small nanoparticles of diameter *ca* <10nm were observed (Fig 6c). EDX reveals a composition $PdS_{1.75}$, which is in line with the sulphur-rich results previously noted but with an increase due to the presences of thiolate capping groups. PXRD of the sample gave no reflections due to the small PdS core, but a large number of low-angle reflections were seen, which, though non-indexable, are presumably from some ordering within the capping agent side-chains. Similar thiolate-capped nanoparticles have been noted by others from the decomposition of $[Pd(SC_{12}H_{25})]_6$ in Ph_2O.[29h]

Conclusions

A systematic crystal structure analysis of $Pd(S_2COR)_2$ of reveals a close similarly of molecular structures and a gradation of crystal packing reliant on directional Pd···S interactions that are usurped by C–H···π(PdS_2C) contacts as the steric bulk of R increases. Computation on **3** (R = *n*-Pr), where the molecular packing features Pd···S, C–H···π(PdS_2C) and C–H···Pd interactions, showed that Pd···S and C–H···π(PdS_2C) interactions are the primary contributors to crystal stability, with non-specific hydrophobic interactions playing a relatively minor role. Specifically, the binding energies in the gas-phase were calculated for the four nearest-neighbour contacts in the crystal, two of which contain clear Pd···S and C–H···π(PdS_2C) and two are non-specific hydrophobic interactions, as revealed by the non-covalent interaction (NCI) plots. The contributions to the stabilisation of the crystal structure were 62.9 and 67.4 kJ/mol for Pd···S and C–H···π(PdS_2C), and 29.9 and 20.9 kJ/mol for the two hydrophobic contacts. As the bulk of R increases, Pd···S interactions are precluded so that the C–H···π(PdS_2C) interactions and hydrophobic contacts increase in significance. The $Pd(S_2COR)_2$ complexes were proved to

function as synthetic precursors for PdS thin films and nanoparticles whereby different compositions, morphologies and sizes could be generated.

Experimental

Synthesis

Details of synthesis, yield, physiochemical and spectroscopic (IR, ^{1}H and ^{13}C{^{1}H} NMR and UV/vis) data are given in ESI Tables S1-S12.

X-ray crystallography

Intensity data were measured at 100 K on an Agilent Technologies SuperNova Dual CCD with an Atlas detector fitted with Mo Kα (λ = 0.71073 Å) or Cu Kα (λ = 1.54184 Å) radiation. Data processing and absorption corrections were accomplished with CrysAlis PRO.[30a] With the use of SHELX programs[30b] integrated into WinGX,[30c] the structures were solved by direct methods and refined on F^2 by full-matrix least-squares with anisotropic displacement parameters for all non-hydrogen atoms. The C-bound H atoms were placed on stereochemical grounds and refined in the riding model approximation with U_{iso} = 1.2-1.5U_{eq}(carrier atom). A weighting scheme of the form $w = 1/[\sigma^2(F_o^2) + (aP)^2 + bP]$ where $P = (F_o^2 + 2F_c^2)/3$ was introduced in each case. For **1**, the (0 1 1) reflection was omitted from the final refinement owing to poor agreement. Several of the refinements exhibited residual electron density peaks greater than 1 e Å^{-3}. For **2**, the maximum and minimum residual electron density peaks of 0.83 and 1.14 e Å^{-3} were located 1.17 and 0.71 from the S1 and Pd atoms, respectively. For **4**, 1.68 and 0.85 e Å^{-3}, respectively, from S2 and Pd atoms; **6**, 0.82 and -1.60 e Å^{-3}, 0.78 and 0.83 Å from Pd; **7**, 1.30 and 3.02 e Å^{-3}, 0.89

and 0.85 Å from Pd; **8**, 1.18 and 1.23 $Å^{-3}$, 0.96 and 0.87 Å from Pd; **10**, 0.91 and 1.05 e $Å^{-3}$, 1.00 and 0.94 Å from Pd; **12**, 4.37 and 2.03 e $Å^{-3}$, 0.96 and 0.89 Å from Pd. Details of unit cell data, X-ray data collection and structure refinement are given in Table 3. The programs ORTEP-3 for Windows,[30c] PLATON[15] and DIAMOND[30d] were also used in the analysis.

Materials chemistry

TEM images were taken using a JEOL JEM 1200EXII Transmission Electron Microscope using an accelerating voltage of 120 kV. EDX measurements were taken using an Oxford INCA Energy X-Ray Analyser. Powder XRD was performed on a Bruker D8 Powder Diffractometer. SEM images were taken on a JEOL JSM 6480LV Scanning Electron Microscope using an accelerating voltage of 15kV.

Aerosol-assisted chemical vapour deposition (AACVD)

All AACVD experiments were performed using a Model 3076 aerosol generator (TSI Inc., Shoreview, MN 5512, USA) and a reaction chamber consisting of a horizontal quartz tube heated by a tube furnace, with precursors **2**, **5**, **6** and **12**. Experiments were performed at 350 °C and 400 °C for a duration of 1 h with a nitrogen carrier gas pressure of 20 psi using *ca* 50 ml of a 0.05M solution of precursor in toluene. The resulting films were analysed by SEM imaging, EDX measurements and PXRD. Substrates used were Si wafer, microscope slides and SiCO-coated float glass from Pilkington / NSG. Substrates cleaned by sonication in propan-2-ol.

Solvothermal Synthesis

Samples (0.25 g) of **7**-**10** in ethylene glycol (50 mL) were heated to reflux in separate experiments and the mixture stirred for 30 min at which point the solution was cooled to room temperature, propan-2-ol (50 mL) added, and the solution centrifuged at 3000 rpm for 10 min. The supernatant was discarded and the process repeated three times to obtain a clean, black powder which was dried *in vacuo*.

Following a literature procedure,[29h] **1** (0.25 g) was dissolved in Ph_2O (45 mL) and dodecanethiol (5 mL), taken to reflux and stirred for 30 min. at that temperature. The same washing method as above was employed.

Acknowledgements

Research in crystal engineering was supported by the High Impact Research MoE Grant UM.C/625/1/HIR/MoE/SC/03 from the Ministry of Higher Education, Malaysia, and the University of Malaya. AOR acknowledges support from the Spanish Malta/Consolider initiative (No. CSD2007-00045) and the Alberta Innovates Technology Futures (AITF) for funding.

References

[1] I. Haiduc, in Comprehensive Coordination Chemistry II, 2004, **1**, 349. J. A. McCleverty and T. J. Meyer (Eds), Elsevier Ltd., Oxford, UK.

[2] (a) P. J. Heard, *Prog. Inorg. Chem.* 2005, **53**, 1; (b) G. Hogarth, *Prog. Inorg. Chem.* 2005, **53**, 71; (c) E. R. T. Tiekink and I. Haiduc, *Prog. Inorg. Chem.* 2005, **54**, 127; (d) I. Haiduc and D. B. Sowerby, *Polyhedron*, 1996, **15**, 2469.

[3] E. R. T. Tiekink, *CrystEngComm*, 2003, **5**, 101; C. S. Lai and E. R. T. Tiekink, *CrystEngComm*, 2003, **5**, 253; E. R. T. Tiekink, *CrystEngComm*, 2006, **8**, 104.

[4] N. N. Adarsh and P. Dastidar, *Chem. Soc. Rev*., 2012, **41**, 3039; M. Dua, C.-P. Lia, C.-S. Liub and S.-M. Fang, *Coord. Chem. Rev*., 2013, **257**, 1282

[5] (a) H. Masui, *Coord. Chem. Rev*., 2001, **219–221**, 957; (b) Y. Z. Wang and G. H. Robinson, *Organometallics*, 2007, **26**, 2; (c) M. K. Milčić, B. D. Ostojić and S. D. Zarić, *Inorg. Chem.*, 2007, **46**, 7109; S. E. Wheeler, *Acc. Chem. Res*., 2013, **46**, 1029; C. I. Yeo, S. N. A. Halim, S. W. Ng, S. L. Tan, J. Zukerman-Schpector, M. A. B. Ferreira and E. R. T. Tiekink, *Chem. Commun.*, 2014, **50**, 5984.

[6] (a) D. Chen, C. S. Lai and E. R. T. Tiekink, *Z. Kristallogr*., 2003, **218**, 747; (b) E. R. T. Tiekink and I. Haiduc, *Prog. Inorg. Chem*., 2005, **54**, 127; (c) E. R. T. Tiekink and J. Zukerman-Schpector, *Chem. Commun*., 2011, **47**, 6623; (d) J. Zukerman-Schpector and E. R. T. Tiekink, *The Importance of Pi-Interactions in Crystal Engineering - Frontiers in Crystal Engineering*, John Wiley & Sons Ltd, Singapore, 2012, ch. 11, pp. 275-299.

[7] *e.g*. G. A. Bogdanović, A. S. Biré and S. D. Zarić, *Eur. J. Inorg. Chem*., 2002, 1599; V. B. Medaković, M. K. Milčić, G. A. Bogdanović and S. D. Zarić, *J. Inorg. Biochem*., 2004, **98**, 1867;; Y.-F. Jiang, C.-J. Xi, Y.-Z. Liu, J. Niclós-Gutiérrez and D. Choquesillo-

Lazarte, *Eur. J. Inorg. Chem*., 2005; V. B. Medakovića, G. A. Bogdanovićb, M. K. Milčića, G. V. Janjićc and S. D. Zarić, *J. Inorg. Biochem*., 2012, **117**, 157; M. V. Câmpian, I. Haiduc and E. R. T. Tiekink, *Z. Kristallogr*. 2013, **228**, 187; S. K. Singh, M. G. B. Drew and N. Singh, *CrystEngComm*, 2013, **15**, 10255; T. S. Basu Baul, S. Kundu, S. W. Ng, N. Guchhait and E. R. T. Tiekink, *J. Coord. Chem*., 2014, **67**, 96; A. N. Gupta, V. Kumar, V. Singh, K. K. Manar, M. G. B. Drew and N. Singh, *CrystEngComm*, 2014, **16**, 9299.

[8] M. K. Milčič, V. B. Medaković, D. N. Sredojević, N. O. Juranić, Z. D. Tomić, S. D. Zarić, *Inorg. Chem*., 2006, **45**, 4755.

[9] A. Nangia, *J. Chem. Sci*., 2010, **122**, 295.

[10] (a) A. Singhal, D. P. Dutta, A. K. Tyagi, S. M. Mobin, P. Mathur and I. Lieberwirth, *J. Organomet. Chem*., 2007, **692**, 5285; (b) W. Friebolin, G. Schilling, M. Zöller and E. Amtmann, *J. Med. Chem*., 2005, **48**, 7925; (c) S. Shahzadi, S. Ali, R. Jabeen and M. K. Khosa, *Turk. J. Chem*., 2009, **33**, 307; (d) I. Ara, F. El Bahij, M. Lachkar, and N. Ben Larbi, *Acta Crystallogr*., *C59*, m199 (2003); (e) Y. Wang, L. Yan, J. Fu and M. Chai, *Huaxue Tongbao*, 2005, **68**, w036; (f) G. V. Romanenko, N. V. Podberezskaya, I. A. Baidina, V. V. Bakakin and S. V. Borisov, *Zh. Strukt. Khim*., 1979, **20**, 520; (g) H. W. Chen and J. P. Fackler, Jr, *Inorg. Chem*., 1978, **17**, 22.

[11] (a) G. Winter, *Rev. Inorg. Chem*., 1980, **2**, 253; (b) S. S. Garje and V. K. Jain, *Coord. Chem. Rev*., 2003, **236**, 35; (c) A. A. Mohamed, I. Kani, A. O. Ramirez and J. P. Fackler, Jr, *Inorg. Chem*., 2004, **43**, 3833.

[12] M. J. Frisch, G. W. Trucks, H. B. Schlegel, G. E. Scuseria, M. A. Robb, J. R. Cheeseman, G. Scalmani, V. Barone, B. Mennucci, G. A. Petersson, H. Nakatsuji, M. Caricato, X. Li,

H. P. Hratchian, A. F. Izmaylov, J. Bloino, G. Zheng, J. L. Sonnenberg, M. Hada, M. Ehara, K. Toyota, R. Fukuda, J. Hasegawa, M. Ishida, T. Nakajima, Y. Honda, O. Kitao, H. Nakai, T. Vreven, J. A. Montgomery Jr., J. E. Peralta, F. Ogliaro, M. Bearpark, J. J. Heyd, E. Brothers, K. N. Kudin, V. N. Staroverov, R. Kobayashi, J. Normand, K. Raghavachari, A. Rendell, J. C. Burant, S. S. Iyengar, J. Tomasi, M. Cossi, N. Rega, J. M. Millam, M. Klene, J. E. Knox, J. B. Cross, V. Bakken, C. Adamo, J. Jaramillo, R. Gomperts, R. E. Stratmann, O. Yazyev, A. J. Austin, R. Cammi, C. Pomelli, J. W. Ochterski, R. L. Martin, K. Morokuma, V. G. Zakrzewski, G. A. Voth, P. Salvador, J. J. Dannenberg, S. Dapprich, A. D. Daniels, Ö. Farkas, J. B. Foresman, J. V. Ortiz, J. Cioslowski and D. J. Fox, *Gaussian 09, Revision A.1*., Gaussian, Inc., Wallingford CT, 2009.

[13] (a) A. D. Becke, *J. Chem. Phys*., 1993, **98**, 5648; (b) C. Lee, W. Yang and R. G. Parr, *Phys. Rev. B*, 1988, **37**, 785; (c) K. A. Peterson and C. Puzzarini, *Theor. Chem. Acc*., 2005, **114**, 283; (d) J. Tomasi, B. Mennucci and R. Cammi, *Chem. Rev*., 2005, **105**, 2999; (e) N. M. O'Boyle, A. L. Tenderholt and K. M. Langner, *J. Comp. Chem*., 2008, **29**, 839.

[14] M. A. Buntine, M. J. Cox, Y. X. Lim, T. C. Yap and E. R. T. Tiekink, *Z. Kristallogr.*, 2003, **218**, 56.

[15] N. W. Alcock, *Adv. Inorg. Chem. Radiochem*., 1972, **15**, 1; I. Haiduc, *Secondary Bonding* in J. L. Atwood and J. Steed (Eds), *Encyclopedia of Supramolecular Chemistry*, Marcel Dekker Inc., New York, 2004, 1215.

[16] (a) A. Bondi, *J. Phys. Chem*., 1964, **68**, 441; (b) C. Janiak, *J. Chem. Soc., Dalton Trans*., 2000, 3885; (c) R. S. Rowland and R. Taylor, *J. Phys. Chem*., 1996, **100**, 7384.

[17] A. L. Spek, *J. Appl. Crystallogr.*, 2003, **36**, 7.

[18] M. Brookhart, M. L. H. Green and G. Parkin, *Proc. Natl. Acad. Sci. USA*, 2007, **104**, 6909; Y. Zhang, J. C. Lewis, R. G. Bergman, J. A. Ellman and E. Oldfield, *Organometallics*, 2006, **25**, 3515; C. Taubmann, K. Ofele, E. Herdtweck and W. A. Herrmann, *Organometallics*, 2009, **28**, 4254; W. Scherer, A. C. Dunbar, J. E. Barquera-Lozada, D. Schmitz, G. Eickerling, D. Kratzert, D. Stalke, A. Lanza, P. Macchi, N. P. M. Casati, J. Ebad-Allah and C. Kuntscher, *Angew. Chem*., 2015, **127**, 2535.

[19] G. Rajput, V. Singh, A. N. Gupta, M. Kumar Yadav, V. Kumar, S. Kumar Singh, A. Prasad, M. G. B. Drew and N. Singh, *CrystEngComm*, 2013, **15**, 4676; S. K. Singh, M. G. B. Drew and N. Singh, *CrystEngComm*, 2013, **15**, 10255; A. N. Gupta, V. Kumar, V. Singh, K. K. Manar, M. G. B. Drew and N. Singh, *CrystEngComm*, 2014, **16**, 9299; V. Kumar, V. Singh, A. N. Gupta, S. K. Singh, M. G. B. Drew and N. Singh, *Polyhedron*, 2015, **89**, 304; V. Kumar, V. Singh, A. N. Gupta, M. G. B. Drew and N. Singh, *Dalton Trans*., 2015, **44**, 1716; S. Poirier, R. J. Roberts, D. Le, D. B. Leznoff and C. Reber, *Inorg. Chem*., 2015, **54**, 3728; M. K. Yadav, G. Rajput, L. B. Prasad, M. G. B. Drew and N. Singh, *New J. Chem*., 2015, **39**, 5493.

[20] E. R. T. Tiekink and J. Zukerman-Schpector, *Aust. J. Chem*., 2010, **63**, 535; J. Zukerman-Schpector, A. Otero-de-la-Roza, V. Luanã and E. R. T. Tiekink, *Chem. Commun*., 2011, **47**, 7608; J. Zukerman-Schpector, I. Haiduc and E. R. T. Tiekink, *Chem. Commun*., 2011, **47**, 12682; J. Zukerman-Schpector, I. Haiduc, E. R. T. Tiekink, *Adv. Organomet. Chem*., 2012, **60**, 49; I. Caracelli, J. Zukerman-Schpector and E. R. T. Tiekink, *Coord. Chem. Rev*., 2012, **256**, 412; I. Caracelli, I. Haiduc, J. Zukerman-Schpector and E. R. T. Tiekink, *Coord. Chem. Rev*., 2013, 257, 2863; J. Zukerman-Schpector and E. R. T. Tiekink,

CrystEngComm, 2014, **16**, 6398; I. Caracelli, I. Haiduc, J. Zukerman-Schpector and E. R. T. Tiekink, *Coord. Chem. Rev.*, 2014, **281**, 50.

[21] C. R. Groom and F. H. Allen, *Angew. Chem. Int. Ed*., 2014, **53**, 662.

[22] A. Mukherjee and G. R. Desiraju, *IUCrJ*, 2014, **1**, 49.

[23] E. R. T. Tiekink, *CrystEngComm*, 2003, **5**, 101; Y. Liu and E. R. T. Tiekink, *CrystEngComm*, 2005, **7**, 20; E. R. T. Tiekink, *CrystEngComm*, 2006, **8**, 104; E. R. T. Tiekink, *Appl. Organomet. Chem*., 2008, **22**, 533; E. R. T. Tiekink and J. Zukerman-Schpector, *Coord. Chem. Rev*., 2010, **254**, 46.

[24] J. D. Dunitz and R. Taylor, *Chem. – Eur. J*., 1997, **3**, 89.

[25] (a) A. D. Becke and E. R. Johnson, *J. Chem. Phys*., 2007, **127**, 154108; (b) A. Otero-de-la-Roza and E. R. Johnson, *J. Chem. Phys*., 2012, **136**, 174109.

[26] (a) A. Otero-de-la-Roza and E. R. Johnson, *J. Chem. Phys*., 2012, **137**, 054103; (b) A. Otero-de-la-Roza and E. R. Johnson, *J. Chem. Phys*., 2013, **138**, 204109; (c) A. Otero-de-la-Roza, J. D. Mallory and E. R. Johnson, *J. Chem. Phys*., 2014, **140**, 18A504.

[27] (a) P. Giannozzi, S. Baroni, N. Bonini, M. Calandra, R. Car, C. Cavazzoni, D. Ceresoli, G. L Chiarotti, M. Cococcioni, I. Dabo, A. Dal Corso, S. de Gironcoli, S. Fabris, G. Fratesi, R. Gebauer, U. Gerstmann, C. Gougoussis, A. Kokalj, M. Lazzeri, L. Martin-Samos, N. Marzari, F. Mauri, R. Mazzarello, S. Paolini, A. Pasquarello, L. Paulatto, C. Sbraccia, S. Scandolo G. Sclauzero, A. P Seitsonen, A. Smogunov, P. Umari1 and R. M Wentzcovitch, *J. Phys.: Condens. Matter*, 2009, **21**, 395502; (b) A. D. Becke, *J. Chem. Phys*., 1986, **85**, 7184; (c) J. P. Perdew, K. Burke and M. Ernzerhof, *Phys. Rev. Lett*., 1996, **77**, 3865.

[28] (a) O. A. Vydrov and G. E. Scuseria, *J. Chem. Phys*., 2006, **125**, 234109; (b) O. A. Vydrov, J. Heyd, A. V. Krukau and G. E. Scuseria, *J. Chem. Phys*., 2006, **125**, 074106; (c) E. R. Johnson, A. Otero-de-la-Roza, S. G. Dale and G. A. DiLabio, *J. Chem. Phys*., 2013, **139**, 214109.

[29] (a) M. P. O'Brien and J Water, *Chem. Vap. Deposition,* 2006, **12**, 620; (b) M. A. Malik, P. O'Brien and N. Revaprasadu, *J. Mater. Chem*. 2002, **12**, 92; (c) A Birri, B Harvey, G Hogarth, E Subasi and F Ugûr, *J. Organomet. Chem*., 2007, **692**, 2448; (d) P. L. Musetha, N. Revaprasadu, G. A. Kolawole, R. V. S. R. Pullabhotla, K. Ramasamy and P. O'Brien, *Thin Solid Films*, 2010, **519**, 197; (e) J. Cheon, D. S. Talaga and J. I. Zink, *Chem. Mater*., 1997, **9***,* 1208; (f) F. Gronvold and E. Rost, *Acta Chem. Scand*., 1956, **10**, 1620; (g) Z. Yang, K. J. Klabunde and C. M. Sorensen, *J. Phys. Chem. C*, 2007, **111***,* 18143; (h) Z. Yang, Ar. B. Smetana, Cr. M. Sorensen and K. J. Klabunde, *Inorg. Chem*., 2007, **46**, 2427.

[30] (a) Agilent Technologies, *CrysAlisPro*. Santa Clara, CA, USA. 2014; (b) G. M. Sheldrick, *Acta Crystallogr*., *Sect. C, Struct. Chem.*, 2015, **71**, 3; (c) L. J. Farrugia, *J. Appl. Crystallogr*., 2012, **45**, 849; (d) *DIAMOND, Visual Crystal Structure Information System, Version 3.1*, CRYSTAL IMPACT, Postfach 1251, D-53002 Bonn, Germany, 2006.

Table 1 Summary of intermolecular interactions (A–H…B; Å, º) operating in the crystal structures of **2**–**12**

A	H	B	A–H	H…B	A…B	A–H…B	Symmetry operation
2							
C2	H2a	Cg(PdS1S2C1)	0.99	2.86	3.672(3)	140	1/2-*x*, 1/2+*y*, *z*
3							
C2	H2a	Cg(PdS1S2C1)	0.99	2.91	3.753(4)	143	2-*x*, 1-*y*, 1-z
C2	H2b	Pd	0.99	2.83	3.759(4)	156	1-*x*, 1-*y*, 1-*z*
4							
C4	H4a	S1	0.98	2.83	3.617(2)	138	½+*x*, ½-*y*, -½+*z*
C2	H2	Cg(PdS1S2C1)	1.00	2.91	3.796(2)	151	½-*x*, ½+*y*, ½-*z*
C4	H4b	Cg(PdS1S2C1)	0.98	2.96	3.845(2)	151	-½+*x*, 1½-*y*, -½+*z*
5							
C2	H2a	S1	0.99	2.87	3.850(2)	170	-1+*x*, *y*, *z*
C2	H2b	Cg(PdS1S2C1)	0.99	2.97	3.873(2)	153	1-*x*, -*y*, 1-*z*
C4	H4b	Cg(PdS1S2C1)	0.99	2.96	3.747(2)	138	*x*, -1+*y*, *z*

6							
C2	H2a	Cg(PdS1S2C1)	0.99	3.11	3.952(3)	144	1+*x*, *y*, *z*
C4	H4a	Cg(PdS1S2C1)	0.99	3.07	3.928(4)	147	1+*x*, *y*, *z*
7							
C2	H2b	Cg(PdS1S2C1)	0.99	2.86	3.779(6)	155	1-*x*, -*y*, 1-*z*
C4	H4b	Cg(PdS1S2C1)	0.99	3.01	3.763(5)	133	*x*, -1+*y*, *z*
8							
C2	H2a	Cg(PdS1S2C1)	0.99	3.11	3.858(3)	134	1-*x*, 2-*y*, 1-*z*
C5	H5a	Cg(PdS1S2C1)	0.98	3.14	3.895(3)	136	*x*, 1+*y*, *z*
9							
C4	H4b	Cg(PdS1S2C1)	0.98	3.09	3.995(2)	155	-1+*x*, *y*, *z*
10							
C2	H2b	Cg(PdS1S2C1)	0.99	2.86	3.739(2)	148	1-*x*, 1-*y*, 1-*z*
C4	H4b	Cg(PdS1S2C1)	0.99	3.08	3.873(2)	153	1-*x*, -*y*, 1-*z*
11							
C2	H2a	Cg(PdS1S2C1)	0.99	2.98	3.9274(17)	160	1-*x*, 1-*y*, 1-*z*
C4	H4a	Cg(PdS1S2C1)	0.99	3.10	3.836(2)	132	-1+*x*, *y*, *z*

12

C2	H2a	Cg(PdS1S2C1)	0.99	3.12	3.826(5)	130	1-*x*, 1-*y*, 1-*z*
C3	H3a	Cg(PdS1S2C1)	0.99	3.06	3.561(5)	113	*x*, -1+*y*, *z*
C3	H3b	Cg(PdS1S2C1)	0.99	3.11	3.561(5)	109	*x*, -1+*y*, *z*

Table 2. Published data on the CVD of palladium sulphide from molecular precursors.

	Pd:S	Method	Substrate	300 °C	350 °C	450 °C	475 °C	475-500 °C	500 °C	525 °C	Ref.
$(\eta^3\text{-}C_3H_5)Pd\{S_2CN(Me)Hex]$	1:2	LPCVD[a]	glass		$Pd_{2.8}S$ + Pd_3S, Pd_4S, $Pd_{2.2}S$, $Pd_{2.5}S$						[29c]
$Pd(S_2CNEt_2)_2$	1:4	AACVD[b]	glass				Pd_4S				[29a]
$Pd[S_2CN(Me)Et]_2$	1:4	AACVD[b]	glass			PdS, $Pd_{16}S_7$					[29a]
$Pd[S_2CN(Me)nBu]_2$	1:4	AACVD[b]	glass			$Pd_{16}S_7$		$Pd_{16}S_7$ + Pd_4S		Pd	[29a]
$Pd[S_2CN(Me)Hex]_2$	1:4	LPCVD[a]	GaAs						PdS		[29a]
$[Pd\{N(iPr_2PS)_2\}_2]$	1:4	LPCVD[a]	glass						PdS_2		[29a, b]
$Pd(S_2COiPr)_2$	1:4	LPCVD[a]	Quartz, Si	PdS							[29e]
$Pd(S_2COiPr)_2$	1:4	PACVD[c]	Quartz, Si	PdS[d]							[29e]

[a] Low-pressure CVD, [b] aerosol-assisted CVD, [c] photo-assisted CVD, [d] T = near sublimation temperature of 105 °C in laser-irradiated regions

Table 3 Crystallographic data and refinement details for **1–12**

Compound	**1**	**2**	**3**	**4**
Formula	$C_4H_6O_2PdS_4$	$C_6H_{10}O_2PdS_4$	$C_8H_{14}O_2PdS_4$	$C_8H_{14}O_2PdS_4$
Formula weight	320.73	348.78	376.83	376.83
Crystal colour	Orange	Orange	Orange	Orange
Crystal size/mm^3	0.05x0.05x0.05	0.05x0.10x0.20	0.07x0.09x0.21	0.19x0.27x0.34
Crystal system	monoclinic	orthorhombic	triclinic	monoclinic
Space group	$P2_1/c$	$Pbca$	$P\bar{1}$	$P2_1/n$
a/Å	6.2713(5)	7.5034(4)	7.4778(4)	9.9077(6)
b/Å	13.5593(11)	7.2125(4)	9.5272(6)	5.8720(3)
c/Å	10.7931(8)	20.7854(12)	9.8084(5)	11.9621(6)
α/°	90	90	74.832(5)	90
β/°	97.635(9)	90	86.458(4)	102.752(5)
γ,/°	90	90	76.292(5)	90
V/Å^3	909.65(12)	1124.87(11)	655.22(7)	678.77(6)
Z	4	4	2	2

D_c/g cm^{-3}	2.342	2.059	1.910	1.844
F(000)	624	688	376	376
μ(MoKα)/mm^{-1}	2.903	–	2.031	1.961
μ(CuKα)/mm^{-1}	–	19.997	–	–
Measured data	4854	9418	5652	5337
θ range/°	3.0 – 27.5	4.3 – 75.0	3.2 – 27.5	3.0 – 27.5
Unique data	2080	1154	3011	1555
Observed data ($I \geq 2.0\sigma(I)$)	1455	1044	2414	1452
No. parameters	102	62	136	72
R, obs. data; all data	0.042; 0.071	0.025; 0.028	0.033; 0.047	0.028; 0.031
a; b in weighting scheme	0.021; 0	0.046; 0	0.029; 0	0.048; 0.292
R_w, obs. data; all data	0.071; 0.083	0.069; 0.072	0.069; 0.077	0.072; 0.074
GoF	1.02	1.13	1.07	1.05
Range of residual electron density peaks/eÅ^{-3}	-0.88 – 0.67	-1.14 – 0.83	-0.97 – 0.93	-0.85 – 1.68

Table 3 *cont.*

Compound	**5**	**6**	**7**	**8**
Formula	$C_{10}H_{18}O_2PdS_4$	$C_{10}H_{18}O_2PdS_4$	$C_{12}H_{22}O_2PdS_4$	$C_{12}H_{22}O_2PdS_4$
Formula weight	404.88	404.88	432.93	432.93
Crystal colour	Yellow	Orange	Orange	Orange
Crystal size/mm^3	0.05x0.05x0.20	0.06x0.11x0.16	0.05x0.10x0.20	0.10x0.20x0.40
Crystal system	triclinic	triclinic	triclinic	triclinic
Space group	$P\bar{1}$	$P\bar{1}$	$P\bar{1}$	$P\bar{1}$
a/Å	5.7038(4)	6.0243(4)	6.8820(11)	6.5622(4)
b/Å	6.7822(4)	8.0461(6)	7.3531(12)	6.8643(5)
c/Å	10.5967(8)	8.9366(7)	10.0455(10)	9.8385(7)
α/°	72.420(6)	111.050(7)	70.305(12)	84.811(6)
β/°	78.467(6)	99.851(6)	70.788(12)	76.424(6)
γ,/°	79.852(5)	103.836(6)	67.164(15)	83.388(6)
V/Å^3	379.94(5)	376.42(5)	429.42(12)	427.00(5)
Z	1	1	1	1

D_c/g cm^{-3}	1.770	1.786	1.674	1.684
F(000)	204	204	220	220
μ(MoKα)/mm^{-1}	1.758	–	–	1.570
μ(CuKα)/mm^{-1}	–	15.036	13.223	–
Measured data	5606	2501	3253	6326
θ range/°	3.2 – 27.5	5.5 – 75.0	6.7 – 75.0	3.0 – 27.5
Unique data	1752	1552	1748	1955
Observed data ($I \geq 2.0\sigma(I)$)	1646	1551	1619	1812
No. parameters	80	81	89	90
R, obs. data; all data	0.024; 0.026	0.028; 0.028	0.054; 0.058	0.029; 0.033
a; b in weighting scheme	0.036; 0.263	0.060; 0.187	0.119; 0.851	0.046; 0.080
R_w, obs. data; all data	0.061; 0.064	0.077; 0.077	0.158; 0.166	0.078; 0.083
GoF	1.10	1.05	1.09	1.13
Range of residual electron density peaks/eÅ^{-3}	-0.82 – 0.98	-1.60 – 0.82	-3.03 – 1.30	-1.23 – 1.18

Table 3 *cont*.

Compound	**9**	**10**	**11**	**12**
Formula	$C_{12}H_{22}O_2PdS_4$	$C_{14}H_{26}O_2PdS_4$	$C_{14}H_{26}O_2PdS_4$	$C_{14}H_{26}O_2PdS_4$
Formula weight	432.93	460.99	460.99	460.99
Crystal colour	Orange	Yellow	Yellow	Yellow
Crystal size/mm^3	0.20x0.30x0.40	0.03x0.20x0.30	0.05x0.20x0.20	0.05x0.10x0.20
Crystal system	triclinic	triclinic	triclinic	triclinic
Space group	$P\bar{1}$	$P\bar{1}$	$P\bar{1}$	$P\bar{1}$
a/Å	6.2746(3)	6.8083(5)	7.0663(5)	6.1398(6)
b/Å	6.3302(4)	7.5446(4)	8.4457(3)	6.7176(5)
c/Å	11.4138(6)	10.4837(8)	9.2536(4)	11.9393(10)
α/°	79.690(5)	101.008(6)	63.740(4)	90.020(7)
β/°	88.152(4)	98.983(6)	73.752(3)	99.397(7)
γ,/°	86.065(5)	112.048(6)	83.782(3)	95.377(7)
V/Å^3	444.89(4)	474.33(6)	475.40(5)	483.63(7)
Z	1	1	1	1

D_c/g cm^{-3}	1.616	1.614	1.610	1.583
F(000)	220	236	236	236
μ(MoKα)/mm^{-1}	1.507	1.419	1.416	–
μ(CuKα)/mm^{-1}	–	–	–	11.778
Measured data	3533	3938	7620	7538
θ range/°	3.3 – 27.5	3.0 – 27.6	3.0 – 27.5	3.8 – 75.0
Unique data	2037	2192	2173	1979
Observed data ($I \geq 2.0\sigma(I)$)	1872	2006	2069	1861
No. parameters	91	98	99	100
R, obs. data; all data	0.023; 0.028	0.029; 0.033	0.017; 0.018	0.056; 0.059
a; b in weighting scheme	0.018; 0	0.023; 0.082	0.021; 0.219	0.130; 0.375
R_w, obs. data; all data	0.047; 0.049	0.064; 0.068	0.042; 0.043	0.158; 0.164
GoF	1.07	1.08	1.04	1.08
Range of residual electron density peaks/eÅ^{-3}	-0.39 – 0.70	-1.05 – 0.91	-0.43 – 0.43	-2.03 – 4.37

Captions to Scheme and Figures

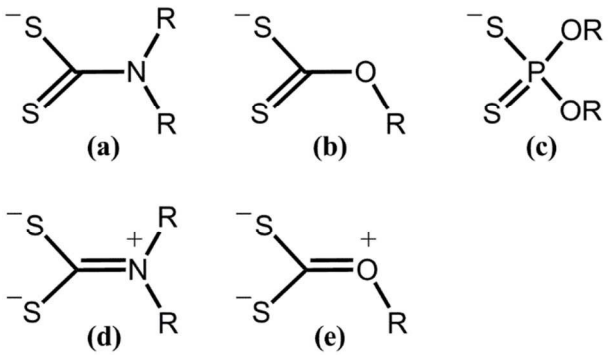

Scheme 1 Generic chemical structures of the (a) dithiocarbamate anion, (b) xanthate anion, (c) dithiophosphate anion, (d) a resonance structure for the dithiocarbamate anion, and (e) a resonance structure for the xanthate anion. R = alkyl/aryl.

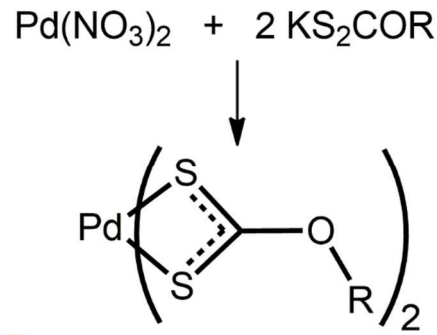

R:

(**1**)	Me	(**7**)	n-Pent
(**2**)	Et	(**8**)	i-Pent
(**3**)	n-Pr	(**9**)	neo-Pent
(**4**)	i-Pr	(**10**)	n-Hex
(**5**)	n-Bu	(**11**)	i-Hex
(**6**)	i-Bu	(**12**)	neo-Hex

Scheme 2 Chemical structures of the palladium(II) bis(xanthate)s (**1**–**12**) investigated herein.

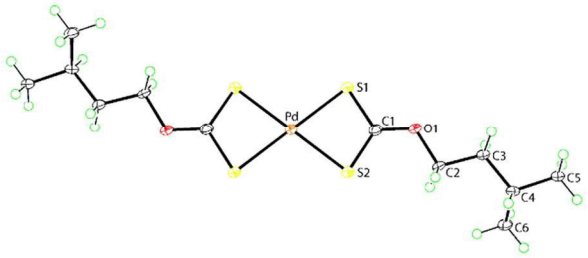

Fig. 1 Molecular structure of **8**, an exemplar of the molecular structures described herein, showing the atom labelling and displacement ellipsoids at the 50% probability level. The molecule is located about a centre of inversion with the unlabelled atoms related by the symmetry operation: 1-*x*, 1-*y*, 1-*z*.

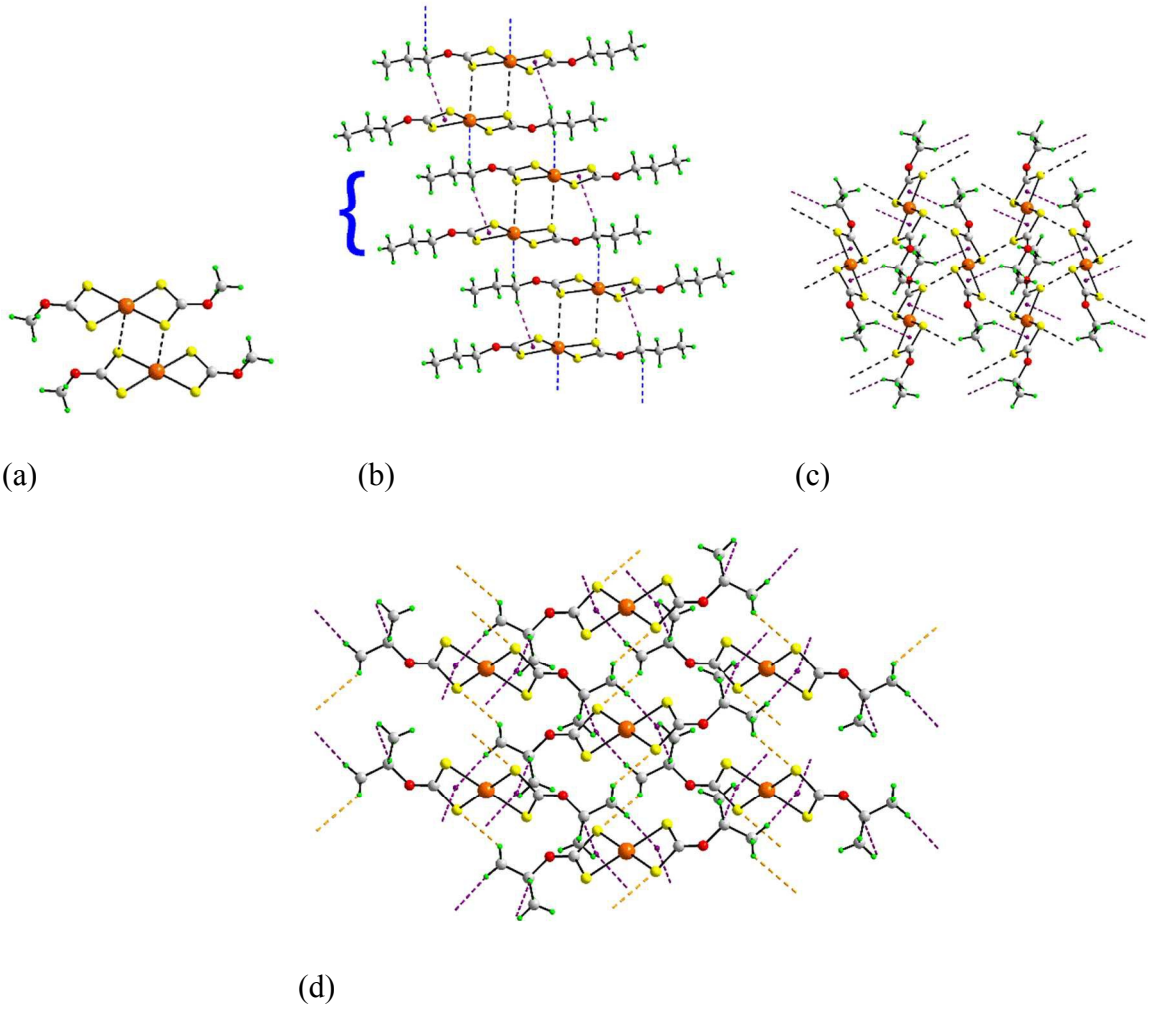

Fig. 2 Supramolecular aggregation in (a) **1**, dimeric aggregate sustained by Pd···S secondary interactions shown as black dashed lines; (b) **3**, supramolecular chain whereby dimeric aggregates, sustained by Pd···S interactions and enclosing C–H···π(PdS_2C) interactions (purple dashed lines), are linked by anagostic C–H···Pd interactions (blue dashed lines). The blue brace highlights one dimeric aggregate; (c) centrosymmetric **2**, supramolecular layer sustained by Pd···S interactions and enclosing two C–H···π(PdS_2C) interactions per molecule; (d) **4**, sustained by C–H···S interactions and enclosing four C–H···π(PdS_2C) interactions per molecule.

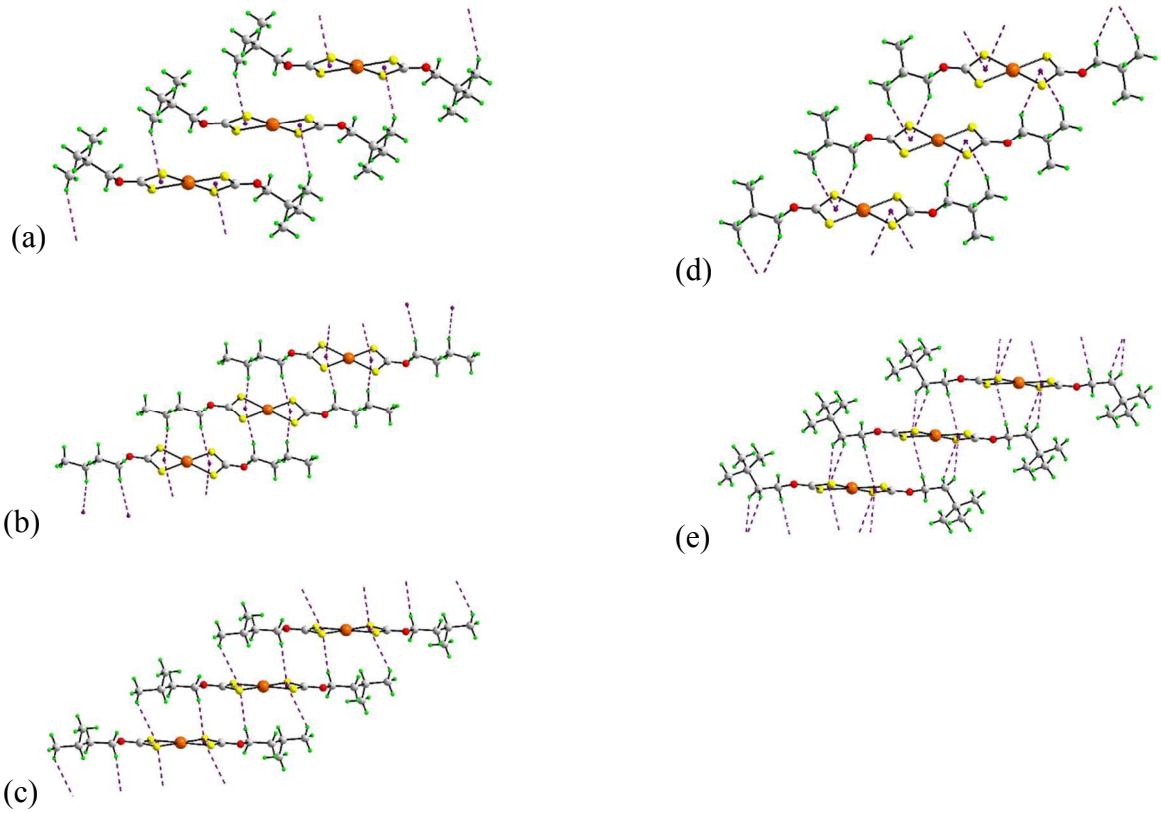

Fig. 3 Supramolecular aggregation in (a) **9**, chains along the *a*-axis sustained by two C–H···π(PdS_2C) interactions per molecule, one per chelate ring and involving methyl-hydrogens; (b) **5**, chains along the *b*-axis sustained by four C–H···π(PdS_2C) interactions per molecule, one on either side of each chelate ring and involving 1,3-related methylene-hydrogens. Similar aggregation is observed in each of **7**, **10** and **11**; (c) **8**, as for **5** but involving 1,4-related methylene- and methyl-hydrogens; (d) **6**, chains along the *a*-axis sustained by four C–H···π(PdS_2C) interactions per molecule, two to one side of each chelate ring and involving 1,3-related methylene- and methyl- hydrogens; and (e) **12**, chains along the *b*-axis sustained by six C–H···π(PdS_2C) interactions per molecule, two to one side and one to the other for each chelate ring and involving 1,2-related methylene-hydrogens.

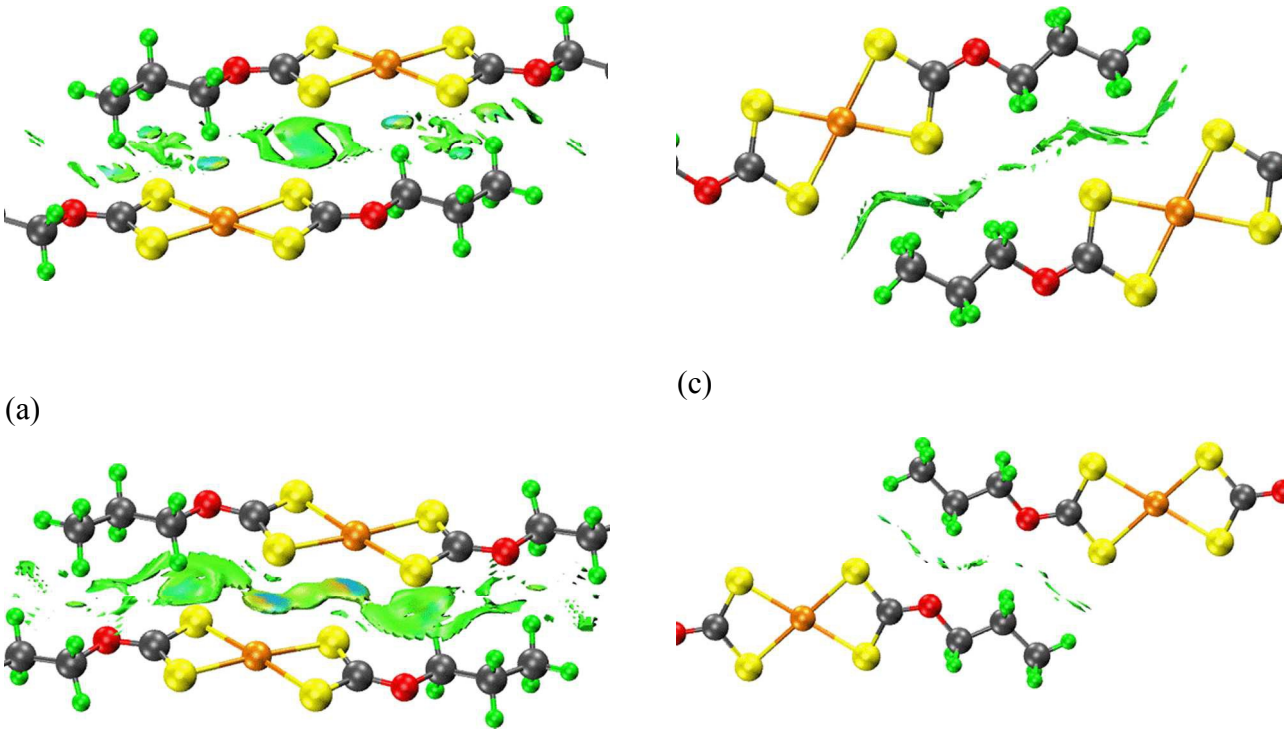

Fig. 4 Non-covalent interaction (NCI) plots in the crystal structure of **3**: a) a stacked contact involving two methylene C–H···π(PdS_2C) interactions, b) a stacked contact with two Pd···S interactions, and (c and d) two distinct side-by-side intermolecular contacts involving the aliphatic substituents.

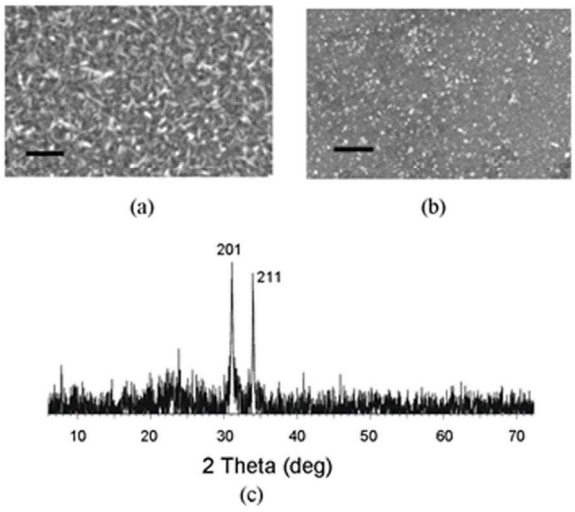

Fig 5 SEM of the films deposited from **2** at 350 ^{o}C: (a) matt section, (b) shiny section (bar = 1 μm for both), (c) PXRD of the film deposited from **6** at 350 ^{o}C (indexed to PdS, PDF 78-0206).

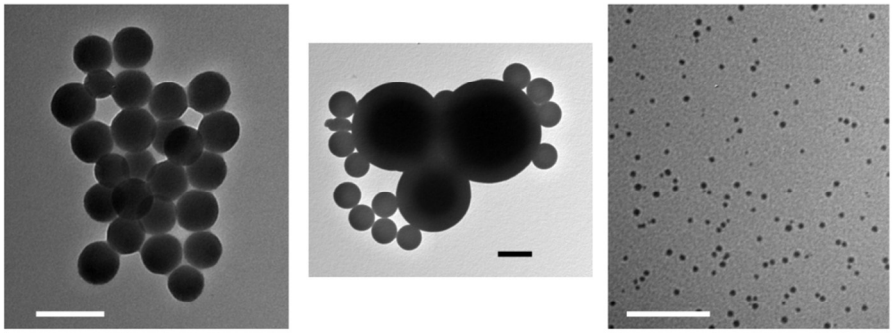

Fig 6. Nanoparticles derived from solvothermal decomposition of (a) **10** (bar = 0.2 μm), (b) **8** (bar = 0.5μm) and (c) **1** (bar = 100nm).

The influence of C–H….π(PdS_2C) interactions in the molecular packing of $Pd(S_2COR)_2$ increases as the steric bulk of *R* increases.